Journal of Electronic Testing (2022) 38:195–203
https://doi.org/10.1007/s10836-022-05998-w

Research on the Mechanical Properties of Magnetorheological Damping and the Performance of Microprobe Test Process

Huajie Huang[1] · Junjie Dai[1] · Long Dou[1] · Junfu Liu[2] · Yunpeng Liu[2] · Taotao Chen[2] · Tianxiang Wu[1] · Junhui Li[1]

Received: 18 October 2021 / Accepted: 29 March 2022 / Published online: 20 April 2022
© The Author(s), under exclusive licence to Springer Science+Business Media, LLC, part of Springer Nature 2022

Abstract
In order to control the stable and controllable loading of the wafer level microprobe test bench, the magnetorheological (MR) damper used in the existing research was optimized and redesigned by introducing intelligent and controllable MR technology. The results show that the MR loading system with optimized structure has good mechanical stability. The mechanical properties of the MR loading system are obtained through the loading current, the loading velocity and the load displacement, etc., and the multi-parameter numerical model of the mechanical system is established, which provides strong support for the development and application of wafer level testing technology, and is also a necessary technical reserve for the development of the new generation of the microelectronics packaging equipment.

Keywords Microprobe test process · Micro-MR damper · Multi-parameter numerical model · Mechanical performance testing · Controllable loading

1 Introduction

With the rapid development of communication technology and mobile phone industry, Moore's Law has been unable to keep up with the development speed of IC, and the packaging technology can further improve the electrical performance of integrated circuits. This is also one of the key research directions of microelectronics manufacturing [18]. Therefore, WLP technology has received a lot of attention in the semiconductor industry. In WLP technology, in order to increase production and reduce costs, the requirements for wafer-level testing are getting higher and higher, and the contact behavior between the probe and the interconnect structure is an important factor affecting the reliability and performance of wafer testing [5].

Because the micro bumps (5–100 microns in diameter) are densely distributed on the wafer, the dynamic impact during the micro-probe test process can easily cause the wafer to rupture [8, 10]. When the contact force between the probe and the interconnect structure is too large, it will create a large probe mark and deformation of the interconnection structure, causing permanent damage to the surface of the wafer. Besides this, excessive mechanical stress may also cause plastic deformation and wear of the probe tip,

Responsible Editor: S. N. Demidenko

✉ Junjie Dai
djj19970210@163.com

✉ Tianxiang Wu
592927171@qq.com

✉ Junhui Li
lijunhui@csu.edu.cn

Huajie Huang
327445442@qq.com

Long Dou
l_doumailbox@126.com

Junfu Liu
liujunfu0110@163.com

Yunpeng Liu
liuyunpeng1990@126.com

Taotao Chen
15256985225@163.com

1 School of Mechanical and Electronical Engineering and State Key Laboratory of High Performance Complex Manufacturing, Central South University, Changsha 410083, China

2 43rd Research Institute China Electronics Technology Group Corporation, Hefei, China

and even cause permanent damage to the probe tip, thereby affecting the test efficiency and lifetime of the probe [13]. However the detected electrical signal may be inaccurate, while the contact force is too small [3, 15, 17]. Accordingly, it is necessary to research on wafer-level probe testing.

In order to improve the accuracy and efficiency of the wafer inspection system, many researchers had done a lot of research on the microprobe. Li et al. [7, 9] designed a final test system of the wafer-level packaging, discussed the influence of the compression displacement and compression speed of the microprobe on the resistance of the probe, studied the dynamic and electrical characteristics of the probe, and proposed the probe lifetime related to the stability of the loading force. Tian et al. [16] studied the real-time electrical characteristics of the microprobe. Lee and Kim [6] studied the influence of the contact position and structure of the probe on its signal transmission characteristics, and found that the outer spring probe has excellent high-frequency characteristics and is suitable for high-speed detection. Basha et al. [2] designed a non-contact electrolyte probe for wafer testing. Nagler et al. [12] proposed a model which can improve the stability of the contact resistance between the IO pad and the probe, and found that the contact resistance has a greater relationship with the shape and roughness of the probe tip. Sia [14] successfully overcame the parasitic resistance between the probe holder and the probe by using the Kelvin test structure. Daffe et al. [4] used a piezoelectric-driven nanopositioner to improve the repeatability of probe positioning. Bahadir [1] had done a lot of work on wafer-level IC testing and test probe cards. These findings would provide an important foundation for microprobe wafer-level final test technology. Since the probe tip and the interconnection structure are in point-to-point contact during the probe test process, it is very important to deepen the understanding of the mechanical properties of the probe.

In this article, a novel miniature MR damper was designed to reduce the possibility of damage to the probe and wafer by using a magnetorheological damper, which acts as a buffer between the wafer and probe, and can achieve flexible loading. The effectiveness of the system was verified by testing the real-time mechanical performance of the system and the results showed that the system had a good stability. Then the experimental data was processed and analyzed, and the model of the stable pressure of the microprobe and multi-parameter were obtained, which provided a reference for future research on the microprobe system.

2 Method and Experiment

The MR damping loading system is shown in Fig. 1. The system consists of a motion control system with a MR damper installed, a pressure acquisition system and a current control system. Microprobe is a kind of pogo pin as shown in Fig. 2a, offered by China Probe Co., Ltd., which has two plungers (Plunger A and Plunger B), a needle and a spring. Figure 2b is the structure diagram of the probe card. It can be seen that the test card consists of five parts: the fixed plate, the PCB board, the probe guide plate, the probe plate and the probes. And the flatness of the test probe card (probe) is 0.02.

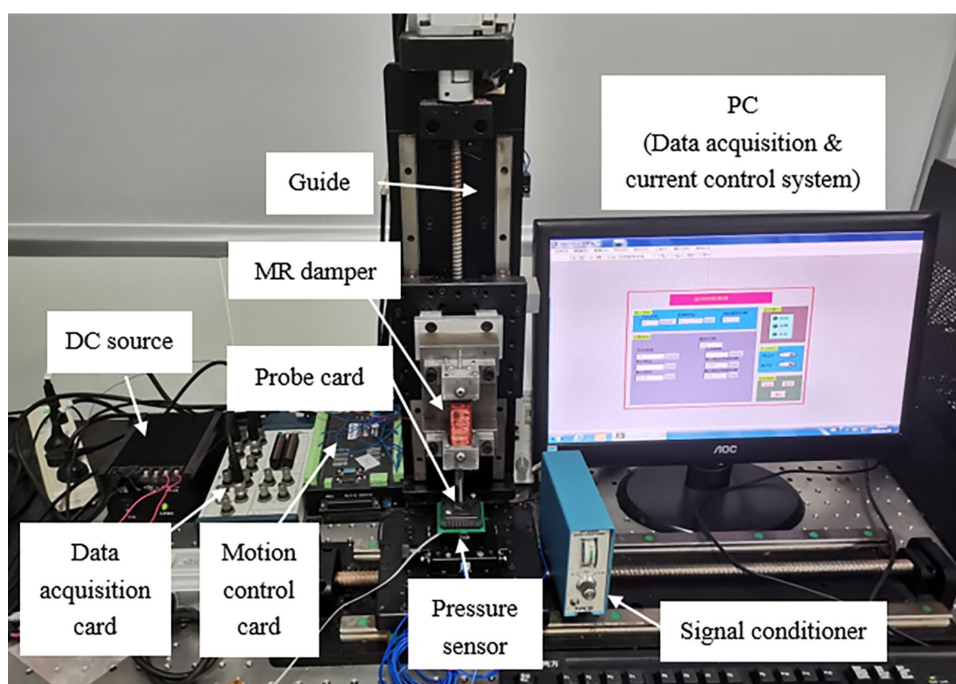

Fig. 1 MR damping loading system

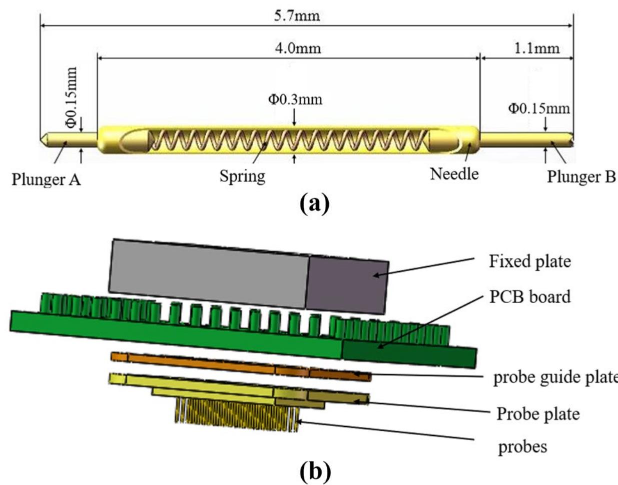

Fig. 2 The structure of the microprobe from (**a**) and the structure of the probe card from (**b**)

The newly designed micro-MR damper has a volume of about 10.6cm^3, which is composed of a square piston rod and cylinder block, and which is different from the circular magnetorheological damper designed by Liu et al. [11]. After the square piston rod and cylinder block are assembled, a pair of interfacing clearance is designed to be 1.5 mm for the flow of damping fluid, and another facing clearance is designed to be 0.05 mm for the restriction of radial rotation. The MR damper is designed to be an external coil winding type with a coil number of 300 turns. The external current is 0-2A and the output pressure is 1-9 N. The MR damper is mounted between the guide rail and the microprobe test card, and driven by the motion control card. The motion control card is made from Shenzhen Lesai Technology Company, China. The model is SMC6480, which belongs to the four-axis motion controller. The pressure sensor and signal conditioner are both manufactured by PCB Piezontronics Inc., and are used in pairs through the connection of signal wires. The data acquisition card is produced by NI Company in the United States, the model is PCI6110. Among them, the sensitivity of the pressure sensor of this brand is 494.604 mV/N (A sensor is used here, and the testing of the wafer requires further study.), and the model of the signal conditioner is 482B11. The displacement of the probe (100–600 μm) is controlled by a drive motor (model A4) produced by Panasonic and its servo motor driver.

In order to establish the first probe electrical contact, we manually adjust the height of the probe to make it contact with the sensor, place FUJIFILM double-layer pressure-sensitive paper on the sensor, and record the position of the probe as "0" when pink appears on the paper. And subsequent electrical contacts add displacement on this basis. In the process of microprobe loading, the collection starts when the acquisition system reaches the trigger value. The pressure signal is read and amplified by the signal conditioner and converted into the corresponding analog voltage signal, which is immediately transmitted to the input end of the data acquisition card and stored and processed at the computer end. After the loading of the microprobe is stable, the approach value oscillating around the stable value is selected as the stable pressure value for analysis. The setting of damping control current and loading parameters can be completed by computer operation.

3 Results and Discussion

3.1 Real-time Pressure Performance

The real-time pressure of the microprobe mainly reflects whether there is a certain degree of stability during the compression process of the contact between the microprobe and the chip when the system is loaded. The pressure stability is beneficial to the reliability of the microprobe test process and results.

Figure 3 are the real-time pressure of the microprobe when the loading speed was 10 mm/s, and each curve in the graph is formed by connecting 2000 single point values. Figure 3a shows the real-time pressure of the microprobe under different damping currents (0-2A) when the loading displacement is 100 μm. It can be seen from the real-time pressure curve that the MR damping loading system has a good stability, and there was no excessive pressure change. Figure 3b shows the real-time pressure of the microprobe when the loading displacement was 600 μm. It can be found that there is a certain fluctuation phenomenon in the pressure value. This is due to the unstable load of the micro-MR damper. And since the output damping force of the magnetorheological damper consists of Coulomb damping force and viscous damping force. When there is no current, the output force is a viscous damping force. When the current is small, the Coulomb damping force is also small, so the output force is not much different from that when there is no current. Thus, the smaller the loading displacement, the better the stability of the pressure.

When the loading speed was 50 mm/s, Fig. 4a and b are the real-time pressures of the microprobes with loading displacements of 100 μm and 600 μm, respectively. The pressure fluctuation range of the MR damping loading system gradually increases, and the increasing law is similar to the loading speed of 10 mm/s.

3.2 The Relationship between Stable Pressure and Loading Displacement

Figure 5a and b correspond to the curves of stable pressure value and loading displacement when the loading speed

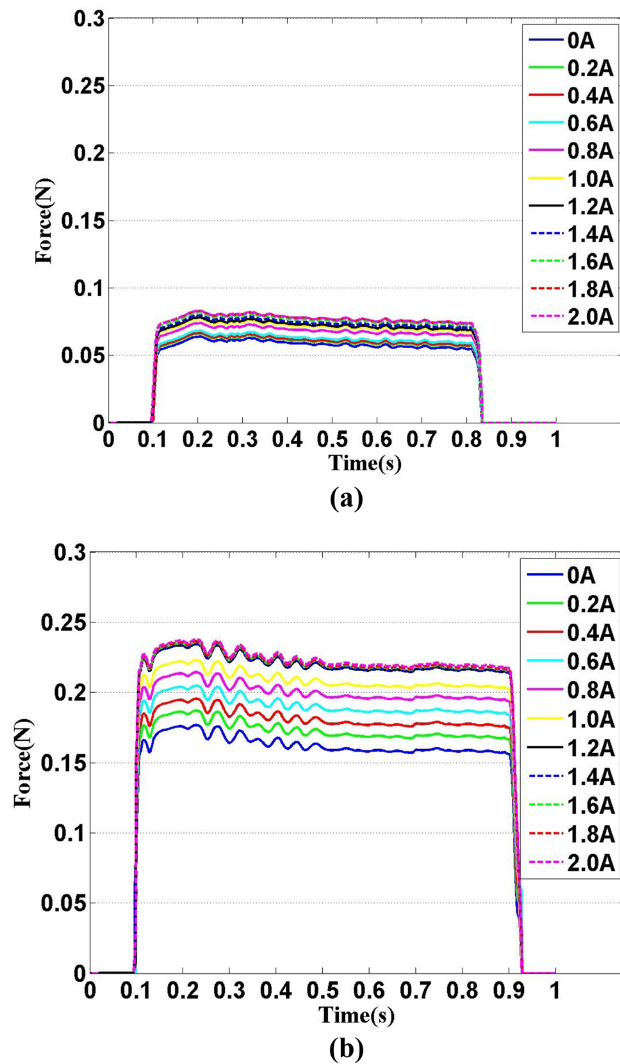

Fig. 3 Real-time pressure curves of the probe when the loading speed was 10 mm/s under current: (**a**) loading displacement was 100 µm; (**b**) loading displacement was 600 µm

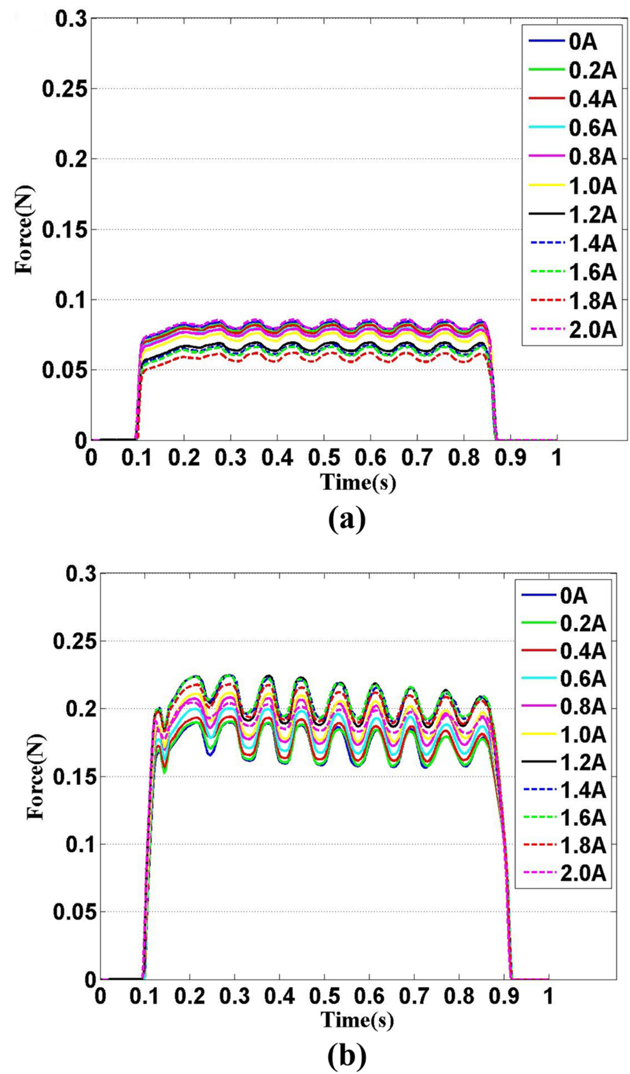

Fig. 4 Real-time pressure curves of the probe when the loading speed was 50 mm/s under current: (**a**) loading displacement was 100 µm; (**b**) loading displacement was 600 µm

were 10 and 50 mm/s, respectively. It can be seen from the figure that the loading displacement corresponds to 100 µm to 600 µm, and each single point value is the average of ten results. As the loading displacement increases, the stable pressure value of the microprobe increases. Generally speaking, in the conditions of 10 mm/s and 50 mm/s loading speed, the change of loading displacement will cause the relative change of the stable pressure, and the loading displacement is an important factor influencing the stable pressure, that is, the greater the loading displacement, the greater the stability pressure. And we can find that the force applied to the probe is only a few tenths of a Newton, which is very small, so the deflection of the system can be ignored.

Figure 5c shows the pressure comparison with and without damper when the loading speed was 10 mm/s. When there is a damper, the pressures are 0.071 N, 0.108 N, and 0.155 N, respectively, and the forces without the damper are 0.107 N, 0.141 N, and 0.172 N. Comparing the results of the experiment, it is found that the test system can effectively reduce the loading pressure of the probe, which has a certain reference significance for realizing the soft landing of the probe loading.

The relationship between the stable pressure of the microprobe and loading displacement is fitted by using the data fitting toolbox of MATLAB software, and the corresponding pressure formulas $F = p1 * x^2 + p2 * x + p3$ (F is the stable pressure and x is the loading displacement. The values of p1, p2 and p3 are shown in Tables 1 and 2) under different conditions are obtained, the fitting curve has 95% confidence level.

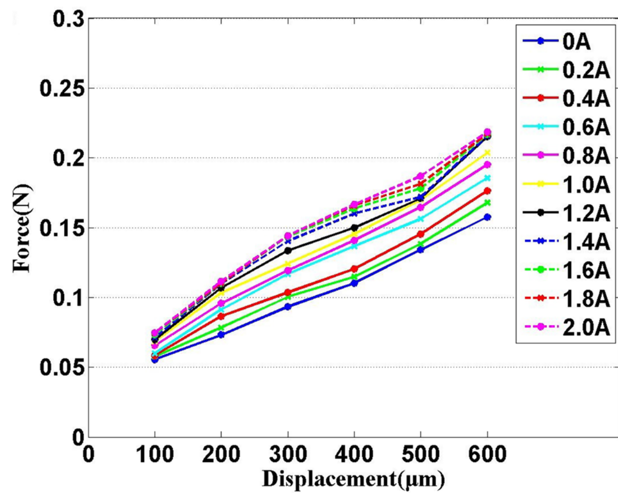

(a)

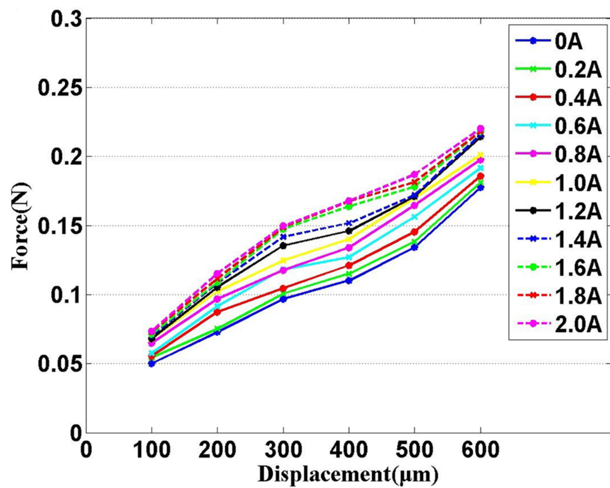

(b)

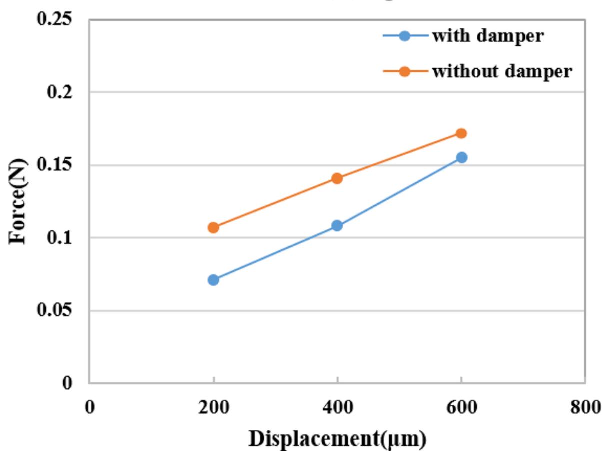

(c)

Fig. 5 The relationship curve between stable pressure and displacement of the microprobe: (**a**) the loading speed was 10 mm/s; (**b**) the loading speed was 50 mm/s; (**c**) the pressure comparison with and without damper when the loading speed was 10 mm/s

Table 1 Fitting parameters of stable pressure and the loading displacement while the loading speed was 10 mm/s

Current(A)	p1	p2	p3
0	7.86E-08	0.0001478	0.04034
0.2	9.07E-08	0.0001495	0.04345
0.4	8.12E-08	0.000167	0.04431
0.6	-6.06E-08	0.0002833	0.03442
0.8	4.91E-09	0.0002469	0.04303
1.0	1.66E-08	0.0002448	0.04757
1.2	2.35E-08	0.0002511	0.04959
1.4	-8.63E-08	0.0003257	0.04395
1.6	-1.19E-07	0.0003523	0.04233
1.8	-1.28E-07	0.0003608	0.04207
2.0	-1.36E-07	0.0003718	0.0409

For example, when the current was 0A and loading displacement was 10 mm/s, it was gotten that

$$F = 7.86 \times 10^{-8}x^2 + 1.478 \times 10^{-4}x + 0.04034 \tag{1}$$

3.3 The Relationship between Stable Pressure and Loading Speed

Figure 6a and b correspond to the relationship between the stable pressure value and the loading speed when the loading displacements are 100 μm and 400 μm, respectively. It can be seen from the figure that as the loading speed increases, the stable pressure value of the microprobe basically tends to be stable. Generally speaking, under the conditions of loading displacements of 100 μm and 400 μm, the change of loading speed has little effect on the stable pressure value of the microprobe.

Table 2 Fitting parameters of stable pressure and the loading displacement while the loading speed was 50 mm/s

Current(A)	p1	p2	p3
0	1.85E-07	0.000109	0.04071
0.2	1.81E-07	0.000113	0.04384
0.4	1.26E-07	0.000153	0.04406
0.6	2.96E-08	0.000229	0.03916
0.8	7.90E-08	0.000197	0.04816
1.0	2.38E-08	0.000236	0.04794
1.2	1.86E-08	0.000255	0.04789
1.4	-4.33E-08	0.000296	0.04633
1.6	-1.53E-07	0.000381	0.03778
1.8	-1.833e-07	0.000401	0.0374
2.0	-1.85E-07	0.000405	0.03833

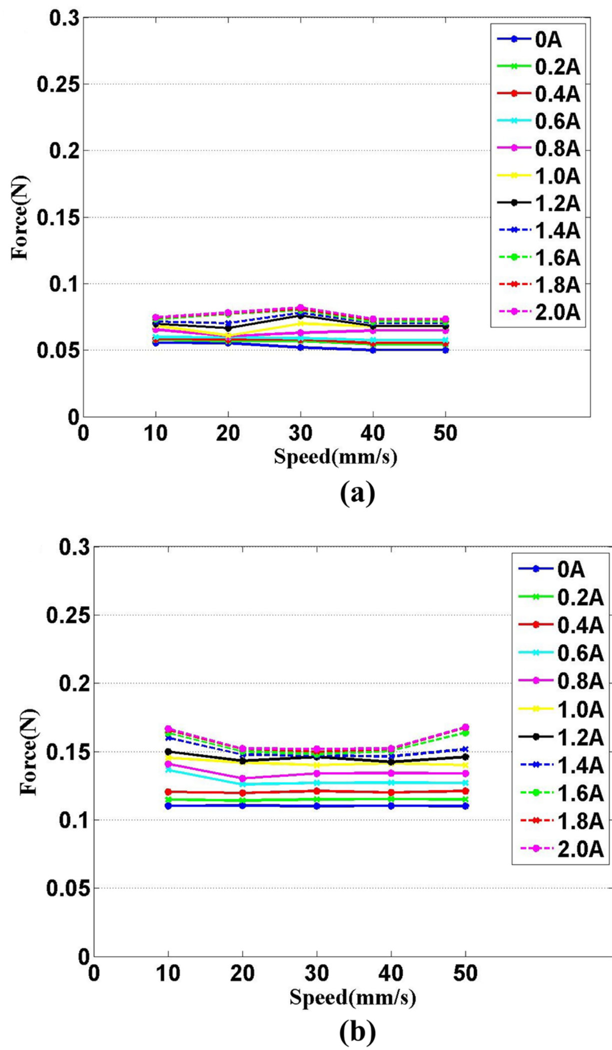

Fig. 6 The relationship between the stable pressure of the microprobe and the loading speed under different loading displacements: (**a**) 100 µm; (**b**) 400 µm

The relationship between the stable pressure of the microprobe and the loading speed is fitted by using the data fitting toolbox of MATLAB software, and the corresponding pressure formulas $F = p1 * v^2 + p2 * v + p3$ (F is the stable pressure and v is the loading speed) under different conditions are obtained, the fitting curve has 95% confidence level.

When the loading displacement were 100 µm and 400 µm, it is shown in Tables 3 and 4 that the parameters p1, p2, and p3 of the fitting formula for the relationship between the stable pressure of the microprobe and the loading speed, and the corresponding loading current were 0-2A (increase every 0.2A).

For example, when the current was 0A and loading displacement was 100 µm, it was gotten that

Table 3 Fitting parameters of stable pressure and the loading speed when the loading displacement was 100 µm

Current(A)	*p1*	*p2*	*p3*
0	1.35E-06	-0.00024	0.05836
0.2	-7.10E-07	-4.99E-05	0.05824
0.4	-1.32E-06	-7.32E-06	0.05866
0.6	-3.00E-07	-4.98E-05	0.06054
0.8	6.77E-06	-0.00038	0.06754
1.0	2.41E-06	-9.24E-05	0.06706
1.2	-7.91E-06	0.00046	0.06464
1.4	-9.43E-06	0.000545	0.06603
1.6	-1.37E-05	0.00072	0.06804
1.8	-1.27E-05	0.00068	0.06944
2.0	-1.39E-05	0.000766	0.0687

$$F = 1.35 \times 10^{-6} v^2 - 2.4 \times 10^{-4} v + 0.05836 \quad (2)$$

3.4 The Relationship between Stable Pressure and Damping Control Current

Figure 7a and b are the relationship between stable pressure and damping control current. The graphs correspond to the curves of stable pressure and damping control current when the loading speed is 10 mm/s and 40 mm/s respectively. It can be seen from the figures that with the increase of the damping control current, the stable pressure value of the microprobe gradually increases, but after the control current reaches 1.6A, the stable pressure value changes very little, and it has basically reached a stable state. Over all, under the condition of damping control current of 0-2A, the stable pressure value increases with the increase of damping control current while the range of damping control current is 0–1.2A. But when the damping control current reaches 1.2A,

Table 4 Fitting parameters of stable pressure and the loading speed when the loading displacement was 400 µm

Current(A)	*p1*	*p2*	*p3*
0	2.06E-05	-0.00125	0.1462
0.2	1.37E-05	-0.00083	0.1463
0.4	1.82E-05	-0.00111	0.1554
0.6	2.29E-05	-0.00138	0.1679
0.8	1.59E-05	-0.00094	0.1716
1.0	8.71E-06	-0.00053	0.1737
1.2	5.79E-06	-0.00036	0.1739
1.4	3.18E-06	-0.00019	0.1734
1.6	7.61E-06	-0.00047	0.1829
1.8	1.47E-05	-0.00088	0.189
2.0	2.99E-05	-0.00179	0.2021

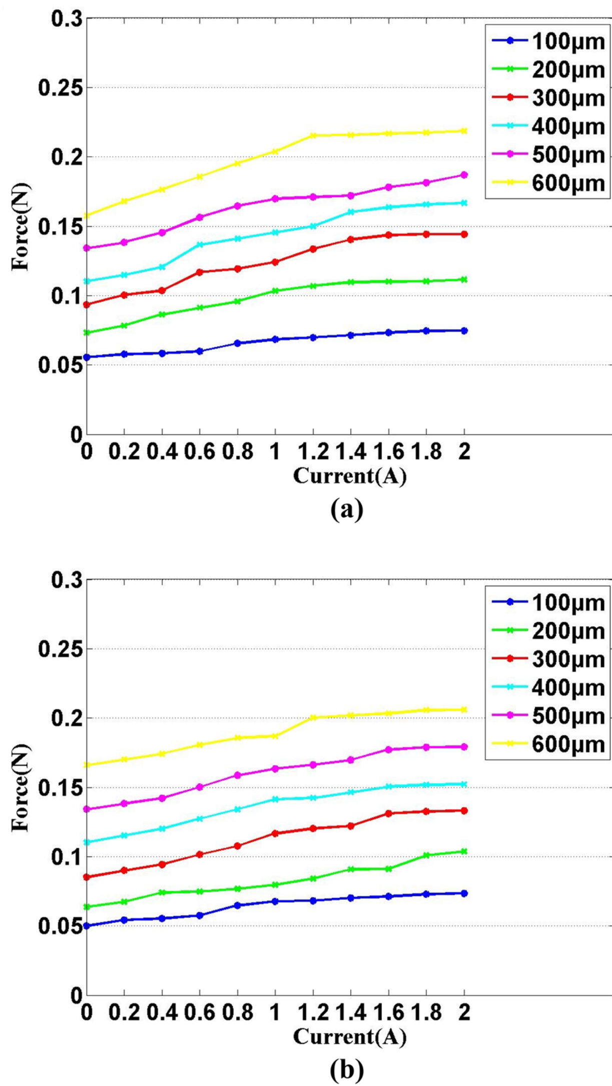

Fig. 7 The relationship between the stable pressure of the microprobe and the damping control current under different loading speeds: (**a**) 10 mm/s; (**b**) 40 mm/s

the increase of damping control current has little effect on the stable pressure because the MR damper is in magnetic saturation state.

The relationship between the stable pressure and the damping control current is fitted by using the data fitting toolbox of MATLAB software, and the corresponding pressure formulas $F = p1 * i^3 + p2 * i^2 + p3 * i + p4$ (F is the stable pressure and i is the damping control current) under different conditions are obtained, the fitting curve has 95% confidence level. It is shown in Table 5 that the parameters p1, p2, p3 and p4 of the fitting formula for the relationship between the stable pressure of the microprobe and the damping control current, while the loading speed were 10 mm/s, and the corresponding loading displacement were 100-600 μm (increase every 100 μm).

Table 5 Fitting parameters of stable pressure while the loading speed was 10 mm/s

Displacement (μm)	*p1*	*p2*	*p3*	*p4*
100	-0.0044	-0.00337	-0.00869	-0.0055
200	0.01106	-0.0003	0.01804	0.0078
300	0.0049	0.03301	0.02396	0.0354
400	0.05556	0.07269	0.0938	0.1089
500	-0.0044	-0.00337	-0.00869	-0.0055
600	0.01106	-0.0003	0.01804	0.0077

For example, when the loading speed was 10 mm/s and loading displacement was 100 μm, it was gotten that

$$F = -4.4 \times 10^{-3} i^3 - 3.37 \times 10^{-3} i^2 - 8.69 \times 10^{-3} i - 5.5 \times 10^{-3} \quad (3)$$

3.5 Effect of Bivariate on the Stable Pressure

Under the combined action of the damping control current and the loading displacement on the stable pressure: it is shown in Fig. 8 that the fitted 3-D surface diagram of the relationship between the stable pressure and the damping control current and the loading displacement, while the loading speed was 10 mm/s.

The fitting mathematical model of the stable pressure, and the damping control current and the loading displacement at the loading speed of 10, 30 and 50 mm/s are shown in the following equations, respectively.

$$F(i,x) = 0.042 - 4.7 \times 10^{-3} i + 1.34 \times 10^{-4} x + 0.011 i^2 + 1.57 \times 10^{-4} ix + 9.61 \times 10^{-8} x^2 - 0.004 i^3 - 1.92 \times 10^{-5} i^2 x - 1.17 \times 10^{-7} ix^2 \quad (4)$$

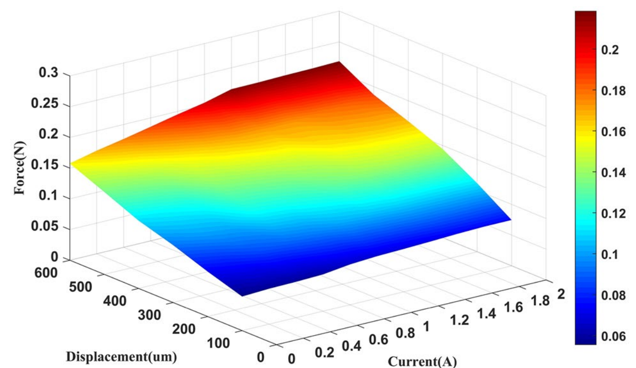

Fig. 8 The fitted 3-D surface diagram of the relationship between the stable pressure and the damping control current and the loading displacement when the loading speed was 10 mm/s

$$F(i,x) = 0.028 - 2.1 \times 10^{-3}i + 2.41 \times 10^{-4}x + 0.024i^2 + 7.66 \times 10^{-5}ix - 1.11 \times 10^{-7}x^2 - 0.007i^3 - 3.77 \times 10^{-5}i^2x + 3.96 \times 10^{-8}ix^2 \quad (5)$$

$$F(i,x) = 0.043 - 1.2 \times 10^{-3}i + 9.21 \times 10^{-5}x + 0.007i^2 + 1.61 \times 10^{-4}ix + 2.05 \times 10^{-7}x^2 - 0.004i^3 - 7.19 \times 10^{-7}i^2x - 1.98 \times 10^{-7}ix^2 \quad (6)$$

Under the combined action of the damping control current and the loading speed on the stable pressure: it is shown in Fig. 9 that the fitted 3-D surface diagram of the relationship between the stable pressure and the damping control current and the loading speed, while the loading displacement was 100 μm.

The fitting mathematical model of the stable pressure, and the damping control current and the loading speed at the loading displacement of 100, 300 and 500 μm are shown in the following equations, respectively.

Under the combined action of the loading speed and the loading displacement on the stable pressure: it is shown in Fig. 10 that the fitted 3-D surface diagram of the relationship between the stable pressure and the loading speed and the loading displacement, while the damping control current was 0A.

The fitting mathematical model of the stable pressure, and the loading speed and the loading displacement at the damping control current of 0A, 1A and 2A are shown in the following equations, respectively.

$$F(i,v) = 0.061 - 8.3 \times 10^{-3}i - 4.17 \times 10^{-4}v + 0.015i^2 + 8.12 \times 10^{-4}iv + 4.34 \times 10^{-6}v^2 - 0.004i^3 - 1.3 \times 10^{-5}i^2v - 8.836 \times 10^{-6}iv^2 \quad (7)$$

$$F(i,v) = 0.0991 - 0.0286i - 6.2 \times 10^{-4}v + 0.0191i^2 + 8.8 \times 10^{-4}iv + 1.05 \times 10^{-5}v^2 - 0.0088i^3 + 4.99 \times 10^{-5}i^2v + 1.358 \times 10^{-5}iv^2 \quad (8)$$

$$F(i,v) = 0.141 - 0.0386i - 9.74 \times 10^{-4}v + 0.003i^2 + 9.15 \times 10^{-5}iv + 1.61 \times 10^{-5}v^2 - 0.002i^3 - 1.96 \times 10^{-6}i^2v - 1.435 \times 10^{-6}iv^2 \quad (9)$$

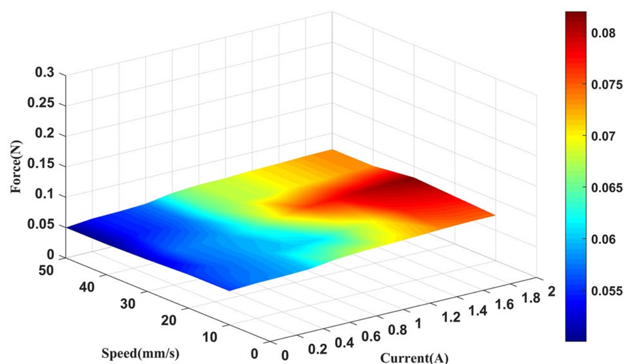

Fig. 9 The fitted 3-D surface diagram of the relationship between the stable pressure and the damping control current and the loading speed when the loading displacement was 100 μm

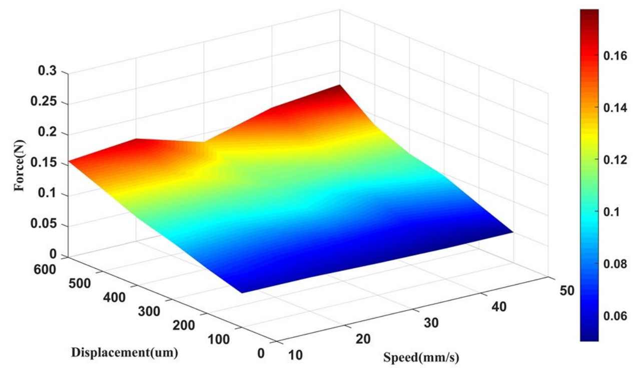

Fig. 10 The fitted 3-D surface diagram of the relationship between the stable pressure and the loading displacement and the loading speed when the damping control current was 0A

$$F(v,x) = 0.056 - 1.22 \times 10^{-3}v - 1.16 \times 10^{-4}x + 1.62 \times 10^{-5}v^2 + 7.99 \times 10^{-7}vx + 1.05 \times 10^{-7}x^2 \quad (10)$$

$$F(v,x) = 0.057 - 1.38 \times 10^{-3}v - 2.26 \times 10^{-4}x + 2.25 \times 10^{-5}v^2 + 9.79 \times 10^{-8}vx + 2.44 \times 10^{-8}x^2 \quad (11)$$

$$F(v,x) = 0.066 - 1.56 \times 10^{-3}v - 3.15 \times 10^{-4}x + 2.62 \times 10^{-5}v^2 + 6.27 \times 10^{-8}vx - 8.49 \times 10^{-8}x^2 \quad (12)$$

4 Conclusion

In summary, experimental verification shows that the micro-MR flexible loading device can effectively limit the radial rotation of the loading process and ensure the stable loading of the system. According to the real-time loading characteristics of the MR loading system during the microprobe test process, data collection and processing are carried out, univariate and bivariate mathematical models are established for the stable pressure, and the mechanical performance characteristics of the system under different parameters are provided as references.

Funding This work was supported by National Natural Science Foundation of China (No. 51975594), National Natural Science Foundation of China joint fund for regional innovation and development (No. U20A6004).

Data Availability The datasets generated during and/or analyzed during the current study are available from the corresponding author on reasonable request.

References

1. Bahadir T (2012) Testing of Copper Pillar Bumps for Wafer Sort. IEEE Trans Compon Packaging Manuf Technol 2(6):985–993
2. Basha MA, Zekrallah A, Abdelkhalek MS, Safavi-Naeini S (2019) A Novel Contactless Dielectric Probe for On-Wafer Testing and Characterization in the V-Band. In: Proc. IEEE-MTT-S International Microwave Symposium (IMS), Boston, MA, pp 1272–1275
3. Chen Y, Xie B, Long J, Kuang Y, Chen X, Hou M, Gao J, Zhou S, Fan B, He Y, Zhang Y, Wong C, Wang Z, Zhao N (2021) Interfacial Laser-Induced Graphene Enabling High-Performance Liquid-Solid Triboelectric Nanogenerator. Adv Mater 33(44):2104290
4. Daffe K, Dambrine G, von Kleist-Retzow F, Haddadi K (2016) RF Wafer Probing with Improved Contact Repeatability Using Nanometer Positioning. In: Proc. 87th ARFTG Microwave Measurement Conference, San Francisco, CA
5. Le XL, Lee HE, Choa S-H (2021) Deformation Behavior of Various Interconnection Structures Using Fine Pitch Microelectromechanical Systems (MEMS) Vertical Probe. J Nanosci Nanotechnol 21(5):2949–2958
6. Lee B-S, Kim M (2018) Effect of Contact Position and Structure of Test Probe on Its Signal Transmission Characteristics. J Korea Acad Ind Coop Soc 19(10):324–329
7. Li J, Liao H, Ge D, Zhou C, Xiao C, Tian Q, Zhu W (2017) An electromechanical model and simulation for test process of the wafer probe. IEEE Trans Ind Electron 64(2):1284–1291
8. Li J, Tian Q, Zhang H, Chen X, Liu X, Zhu W (2018) Study on dipping mathematical models for the solder flip-chip bonding in microelectronics packaging. IEEE Trans Industr Inform 14(11):4746–4754
9. Li J, Tian W, Liao H, Zhou C, Liu X, Zhu W (2017) The mathematical model and novel final test system for wafer-level packaging. IEEE Trans Ind Informat 13(4):1817–1824
10. Li J, Zhang X, Zhou C, Zheng J, Ge D, Zhu W (2016) New applications of an automated system for high-power LEDs. IEEE ASME Trans Mechatron 21(2):1035–1042
11. Liu Y, Xiao J, Li J (2020) Characterization of a probe test system with micro-magnetorheological flexible loading. IEEE Trans Compon Packaging Manuf Technol 10(10):1666–1673
12. Nagler O, Krebs T, Heuken M (2019) An Improved Model of Electrical Contact Resistance of Pad-Probe Interaction during Wafer Test. In: Proc. IEEE Holm Conference on Electrical Contacts, Milwaukee, WI, pp 68–75
13. Sertel K (2019) Automated Performance of On-wafer Calibration and Characterization Using Non-contact Probes. In: Proc. 92nd ARFTG Microwave Measurement Conference (ARFTG), Orlando, FL
14. Sia CB (2017) True Kelvin CMOS Test Structure to achieve Accurate and Repeatable DC Wafer-Level Measurements for Device Modelling Applications. In: Proc. International Conference on Microelectronic Test Structures (ICMTS), Grenoble, France
15. Sun B, Wen CY, Wu RB (2011) A New Isolation Structure of pogo Pins for Crosstalk Reduction in a Test Socket. IEEE Trans Compon Packaging Manuf Technol 1(4):586–594
16. Tian Q, Yuan Q, Wei X, Li J (2018) Real-time electrical characteristics of microprobe testing process in microelectronics packaging. IEEE Trans Semicond Manuf 31(1):166–172
17. Tunaboylu B (2014) Electrical Characterization of Test Sockets With Novel Contactors. IEEE Trans Device Mater Reliab 14(1):580–582
18. Zhou C, Li J, Duan J, Deng G (2016) Control and jetting characteristics of an innovative jet valve with zoom mechanism and opening electromagnetic drive. IEEE ASME Trans Mechatron 21(2):1185–1188

Publisher's Note Springer Nature remains neutral with regard to jurisdictional claims in published maps and institutional affiliations.

Huajie Huang is a master's degree student in Central South University, Changsha, China

Junjie Dai is a master's degree student in Central South University, Changsha, China.

Long Dou is a PhD student in Central South University, Changsha, China.

Junfu Liu is an engineer in the 43rd Research Institute China Electronics Technology Group Corporation, Hefei, China.

Yunpeng Liu is an engineer in the 43rd Research Institute China Electronics Technology Group Corporation, Hefei, China.

Taotao Chen is an engineer in the 43rd Research Institute China Electronics Technology Group Corporation, Hefei China.

Tianxiang Wu is a PhD student in Central South University, Changsha, China.

Junhui Li was born in Taojiang, China, in 1969. He received PhD degree in mechanical engineering from Central South University (CSU), Changsha, China, in 2008. He has been a professor with CSU, since September 2011. He is currently working on electronics packaging. He has published more than 80 papers. His research interests include electronics packaging and manufacturing.